Appl. Math. Mech. -Engl. Ed., **43**(6), 931–944 (2022)

APPLIED MATHEMATICS AND MECHANICS (ENGLISH EDITION)

https://doi.org/10.1007/s10483-022-2854-6

Performance enhancement of a DC-operated micropump with electroosmosis in a hybrid nanofluid: fractional Cattaneo heat flux problem*

A. M. ALSHARIF[1], A. I. ABDELLATEEF[2], Y. A. ELMABOUD[3,4], S. I. ABDELSALAM[5,†]

1. Department of Mathematics and Statistics, College of Science, Taif University, P. O. Box 11099, Taif 21944, Saudi Arabia;
2. Department of Applied Mathematics and Science, Faculty of Engineering, National University of Science and Technology, Seeb 111, Sultanate of Oman;
3. Department of Mathematics, College of Science and Arts at Khulis, University of Jeddah, Jeddah 21589, Saudi Arabia;
4. Department of Mathematics, Faculty of Science, Al-Azhar University (Assiut Branch), Assiut 71254, Egypt;
5. Department of Basic Science, Faculty of Engineering, The British University in Egypt, Cairo 11837, Egypt

(Received Jan. 7, 2022 / Revised Mar. 22, 2022)

Abstract The purpose of this investigation is to theoretically shed some light on the effect of the unsteady electroosmotic flow (EOF) of an incompressible fractional second-grade fluid with low-dense mixtures of two spherical nanoparticles, copper, and titanium. The flow of the hybrid nanofluid takes place through a vertical micro-channel. A fractional Cattaneo model with heat conduction is considered. For the DC-operated micropump, the Lorentz force is responsible for the pressure difference through the microchannel. The Debye-Hükel approximation is utilized to linearize the charge density. The semi-analytical solutions for the velocity and heat equations are obtained with the Laplace and finite Fourier sine transforms and their numerical inverses. In addition to the analytical procedures, a numerical algorithm based on the finite difference method is introduced for the given domain. A comparison between the two solutions is presented. The variations of the velocity heat transfer against the enhancements in the pertinent parameters are thoroughly investigated graphically. It is noticed that the fractional-order parameter provides a crucial memory effect on the fluid and temperature fields. The present work has theoretical implications for biofluid-based microfluidic transport systems.

Key words hybrid nanofluid, fractional Cattaneo heat flux, Caputo-Fabrizio derivative

* Citation: ALSHARIF, A. M., ABDELLATEEF, A. I., ELMABOUD, Y. A., and ABDELSALAM, S. I. Performance enhancement of a DC-operated micropump with electroosmosis in a hybrid nanofluid: fractional Cattaneo heat flux problem. *Applied Mathematics and Mechanics* (*English Edition*), **43**(6), 931–944 (2022) https://doi.org/10.1007/s10483-022-2854-6

† Corresponding author, E-mail: sara.abdelsalam@bue.edu.eg

Chinese Library Classification O363.2
2010 Mathematics Subject Classification 76W05, 76D45

1 Introduction

Electroosmosis is a significant study topic because of its wide applications, e.g., nanodevices in biochemical, medical, and industrial sectors[1]. An electric double layer (EDL) is formed and bonded to an exterior diffused layer inside the charged sheet. When an external power supply field is applied to the EDL, the molecules in the dispersed area of the EDL move to produce mass liquid dislocation via the dense effect, which is also known as the electroosmotic flow (EOF). Many Newtonian and non-Newtonian flows in micro- and nano-fluidic applications are governed by the electroosmosis concept. Zhao et al.[2] studied the EOF of a nanofluid in the magnetic field through a horizontal microchannel, and observed that the magnetic field and EDL had a high effect on the flow and heat transfer. Awan et al.[3] studied the slip effect along with the EOF for a second-grade fluid with the Caputo-Fabrizio fractional derivative, and found out that the velocity field was enhanced with an increase in the fractional parameter. Alsharif and Abd-Elmaboud[4] investigated the fractional Cattaneo model for a fractional second-grade fluid with the EOF, and concluded that the free convectional force was enhanced by the EOF. Abdellateef et al.[5] studied a second-grade factional fluid with the Cattaneo heat flux through a microchannel with the consideration of the EOF, and observed that the time required for the flow rate to get to a steady state increased for the non-Newtonian case.

In recent decades, the fractional derivative models for non-Newtonian fluids have shown to be an excellent technique for assessing the viscoelastic behavior of the flow amount in microfluidic devices. The long-term memory effect of the fractional derivatives is extremely suited and reliable for application. In steady flows, the fluid flow described by the fractional rate of deformation displays a time dependent behavior. Dey and Shit[6] studied the second-grade viscoelastic behavior with the imposed electric field and applied magnetic field, and concluded that the EOF had an increasing effect on the heat transfer rate. Wang et al.[7] analyzed the fractional flows with the EOF through parallel plates with the zeta potentials and pressure gradient by means of the Debye-Hükel approximation, Laplace transforms, and finite difference method. Wang et al.[8] derived the exact solution to a generalized problem of a second-grade flow by means of the integral transform method, considering the fractional derivative. Under the Debye-Hükel approximation, they concluded that there was a monotonous increase in the velocity profile with an increase in the Debye-Hükel parameter. There are many works that shed light on the EOF, micropumps, and nanofluids, e.g., Refs. [9]–[12] and the references therein.

The heat flux system based on the Fourier law is said to be appropriate for most engineering purposes even though it assumes an unlimited propagation speed of thermal perturbations. Nevertheless, under low temperature or rapid heating settings, it fails to predict the temperature accurately. As a result, many non-Fourier models have been developed to address these shortcomings in the analyses for heat transfer characteristics. Qi et al.[13] studied the heat of short laser pulse with the fractional Cattaneo model, and obtained the analytic solutions for the temperature profile by means of Laplace transformations. They deduced that there was a prominent increase in the temperature distribution near to the input pulse ending with an increase in the fractional parameter. Xu and Wang[14] investigated the heat transfer with short pulsed laser in a finite slab for a fractional Cattaneo system. They concluded that enhancing the relaxation time reduced the heat flux propagation. Xu et al.[15] studied a generalized Cattaneo model with non-Fourier heat conduction, and derived the exact solutions by means of Laplace transformations. They concluded that the temperature achieved at the boundary was higher for the Cataneo model than for the fractional Cattaneo model. The Cattaneo-Christov heat flux model has been used in medicinal and bioengineering procedures such as the heat reduction in nuclear reactors and hybrid power generators. Many authors used this model in

their studies because of its wide applicability in heat transport mechanisms[16–18].

The high thermal conductivity at low nanoparticle aggregation, minimum clogging in flow passageways, and long-term stability are all characteristics of nanofluids. These distinguishing characteristics make them more helpful in many applications such as micro-electromechanical systems and cooling of microchips[19–21]. However, the thermal conductivity and long-term stability increase when different nanoparticles are mixed in the base fluid, which is known as "hybrid nanofluid". Due to the importance of this type of fluid, many researchers have studied the flow of hybrid nanofluids in various geometries. Khan et al.[22] discussed the problem of the thermal boundary layer flow of a hybrid nanofluid. They found that the heat transfer augmented due to the elevation of the nanoparticle's volume fraction. Christopher et al.[23] studied the effect of the Catteno-Christov heat flux model on a hybrid nanofluid flow through a porous medium. El-Masry et al.[24] investigated the direct current (DC)/alternating current (AC) MHD micropump of the hybrid nanofluid in the annular region between vertical coaxial microtubes. They concluded that the stream was enhanced by the large concentration of particles in the mixture, resulting in a low necessary pressure.

In light of the efficacy of the fractional models in heat conduction along with the applications of the EOF with non-Newtonian models, we intend to shed light on the EOF of a hybrid nanofluid with copper and titanium nanoparticles through a vertical micro-channel. We fractionalize the proposed model, use the Caputo-Fabrizio derivative, and derive the velocity field with the aid of the Laplace transformation method for the fractional derivative. The Debye-Hükel approximation is utilized to linearize the charge density. The numerical algorithm is introduced, and the analytical and numerical solutions are compared. Graphs are presented to show a clear visualization for the obtained solutions.

2 Problem formulation and mathematical model

The unsteady fractional second-grade fluid flow through a vertical microchannel with the fractional Cattaneo model of heat conduction is considered. The electroosmosis phenomenon is considered. The asymmetric zeta potentials ζ_1 and ζ_2 of the channel walls are constant. The walls are kept at the constant temperatures T_1 and T_2 (see Fig. 1). The fluid is exposed to a uniform magnetic field $\boldsymbol{B} = (0, B_y, 0)$ and an electric field $\boldsymbol{E} = (E_x, 0, -E_z)$. In our manuscript, we will assume the following assumptions.

(i) The Debye-Hükel approximation is used, and hence the following linearized charge density is taken:

$$\varrho_e' = \frac{-2z_i^2 e_i^2 n_0 \Psi'}{d_e T_A B_c}.$$

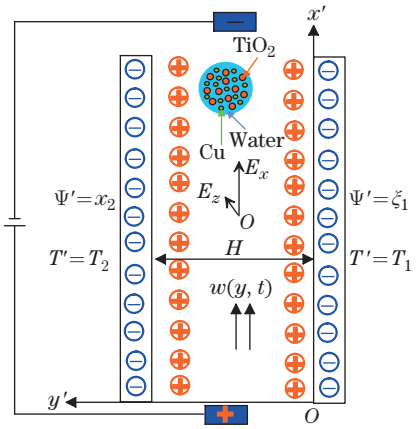

Fig. 1 Geometry of the problem (color online)

(ii) The electroosmotic velocity is assumed to be $\boldsymbol{u}' = u'(y,t)\boldsymbol{i}$.

(iii) In addition to the electroosmotic force, in case of DC-operated magneto-hydrodynamics (MHD), the Lorentz force is responsible for the pressure difference through the microchannel. Therefore, $-P'_x = \boldsymbol{J}' \times \boldsymbol{B} = \big(\sigma\big(B_y E_z - B_y^2 u'\big),\ 0,\ \sigma B_y E_x\big)$, where $\boldsymbol{J}' = \sigma(\boldsymbol{E}' + \boldsymbol{u}' \times \boldsymbol{B})$, T_A is the electrolytic solution temperature, B_{c} is a constant of Boltzmann, e_i is the electron charge, n_0 denotes the ionic concentration in the bulk phase, d_e denotes the solution's dielectric constant, $\boldsymbol{J}'$ is the electric current density, and σ is the electrical conductivity.

The constitutive relations for the fractional second-grade fluid and the fractional Cattaneo model for heat conduction are as follows[4–5,25]:

$$\tau = (\mu_{\mathrm{hnf}} + M_1 \mathfrak{D}_t^{\epsilon})\gamma(t), \quad 0 < \epsilon < 1, \tag{1}$$

$$\Big(1 + \frac{\lambda_2^c}{c!}\mathfrak{D}_t^c\Big)\boldsymbol{q} = -K_{\mathrm{hnf}}\nabla T', \quad 0 < c < 1, \tag{2}$$

where τ is the shear stress, $\boldsymbol{q}$ is heat flux, T' is the temperature, γ is the shear strain, μ_{hnf} is the viscosity of the hybrid nanofluid, M_1 is the viscoelastic constant, K_{hnf} is the thermal conductivity of the hybrid nanofluid, and ϵ and c are the fractional orders.

The time fractional derivative of order ε for the Caputo-Fabrizio model is[26]

$$\mathfrak{D}_t^{\epsilon} g(t) = \frac{L^*(\epsilon)}{1-\epsilon}\int_0^t g'(t)\mathrm{e}^{\frac{\epsilon(t-\tau)}{\epsilon-1}}\,\mathrm{d}\tau, \quad 0 < \epsilon < 1, \tag{3}$$

where $L^*(0) = L^*(1) = 1$. The continuity, momentum, and energy equations, by using the above assumptions, will be[24–25]

$$\frac{\partial u'}{\partial x'} = 0, \tag{4}$$

$$\rho_{\mathrm{hnf}}\frac{\partial u'}{\partial t'} = \frac{\partial \tau'_{xy}}{\partial y'} + \sigma B_y E_z - \sigma B_y^2 u' + \rho'_e E_x + (\rho\,\alpha)_{\mathrm{hnf}} g(T' - T_0), \tag{5}$$

$$(\rho c_p)_{\mathrm{hnf}}\Big(1 + \frac{\lambda'^c}{c!}\frac{\partial^c}{\partial t'^c}\Big)\frac{\partial T'}{\partial t'} = K_{\mathrm{hnf}}\frac{\partial^2 T'}{\partial y'^2} + Q_0\Big(1 + \frac{\lambda'^c}{c!}\frac{\partial^c}{\partial t'^c}\Big)(T' - T_0), \tag{6}$$

where Q_0 is the heat source.

The properties of the hybrid nanofluid are summarized as follows[24]. The density of the hybrid nanofluid is designated by

$$\rho_{\mathrm{hnf}} = \phi_{s_1}\rho_{s_1} + \phi_{s_2}\rho_{s_2} + (1 - \phi_{\mathrm{T}})\rho_{\mathrm{water}}, \tag{7}$$

where $\phi_{\mathrm{T}} = \phi_{s_1} + \phi_{s_2}$ is the overall volume concentration. The viscosity of the hybrid nanofluid is

$$\mu_{\mathrm{hnf}} = \mu_{\mathrm{f}}(1 - \phi_{\mathrm{T}})^{-2.5}. \tag{8}$$

The heat capacitance is

$$(\rho c_p)_{\mathrm{hnf}} = \phi_{s_1}\rho_{s_1}(c_p)_{s_1} + \phi_{s_2}\rho_{s_2}(c_p)_{s_2} + (1 - \phi_{\mathrm{T}})(\rho c_p)_{\mathrm{water}}. \tag{9}$$

The coefficient of thermal expansion is

$$(\rho\alpha)_{\mathrm{hnf}} = (\phi\rho\alpha)_{s_1} + (\phi\rho\alpha)_{s_2} + (1 - \phi_{\mathrm{T}})(\rho\alpha)_{\mathrm{water}}. \tag{10}$$

For low dense mixtures of two substances ($s_1 = \mathrm{Cu}$ and $s_2 = \mathrm{TiO_2}$) with spherical particles, the effective thermal conductivity, according to the Maxwell model, is represented by

$$\frac{K_{\mathrm{hnf}}}{K_{\mathrm{water}}} = \frac{K_{\mathrm{hp}} + 2K_{\mathrm{water}} - 2\phi_{\mathrm{T}}(K_{\mathrm{water}} - K_{\mathrm{hp}})}{K_{\mathrm{hp}} + 2K_{\mathrm{water}} + \phi_{\mathrm{T}}(K_{\mathrm{water}} - K_{\mathrm{hp}})}, \tag{11}$$

where

$$K_{\mathrm{hp}} = \frac{\phi_{s_1} K_{s_1} + \phi_{s_2} K_{s_2}}{\phi_{\mathrm{T}}}.$$

The Debye-Hükel approximation can be applied, and the Poisson equation combining Ψ' and ϱ'_e can be expressed as

$$\nabla^2 \Psi' = \Upsilon'^2 \Psi' = \frac{-\varrho'_e}{\varepsilon}, \tag{12}$$

where $\Upsilon'^2 = \frac{2e^2 n_0 z_v^2}{\varepsilon T_A B_c}$. The boundary and initial conditions are

$$\begin{cases} u'(y',t') = T'(y',t') = 0 \quad \text{at} \quad t' = 0, \\ \Psi'(y') = \zeta_1, \quad u'(y',t') = 0, \quad T'(y',t') = T_0 \quad \text{at} \quad y' = 0, \\ \Psi'(y') = \zeta_2, \quad u'(y',t') = 0, \quad T'(y',t') = T_1 \quad \text{at} \quad y' = H. \end{cases} \tag{13}$$

From Eq. (1), the stress tensor component τ'_{xy} for the small deformation of the viscoelastic fluid can be expressed as

$$\tau'_{xy} = \mu_{\mathrm{hnf}} (1 + \delta \mathfrak{D}_t^{\epsilon}) \frac{\partial u'}{\partial y'}, \tag{14}$$

where δ is the non-Newtonian parameter.

We introduce the following dimensionless variables:

$$\begin{cases} \Psi = \dfrac{\Psi'}{\zeta_1}, \quad u = \dfrac{u'}{u_{\mathrm{HS}}}, \quad y = \dfrac{y'}{H}, \quad t = \dfrac{\mu t'}{H^2 \rho}, \quad \Upsilon = H\Upsilon', \\ \rho_e = -\dfrac{H^2 \varrho'_e}{\zeta_1 \varepsilon}, \quad \eta = \dfrac{\delta}{\mu \left(\frac{H^2 \rho}{\mu}\right)^{\gamma}}, \quad \lambda = \dfrac{\lambda'}{c! (\frac{H^2 \rho}{\mu})^c}, \quad \theta = \dfrac{T' - T_0}{T_1 - T_0}. \end{cases} \tag{15}$$

The non-dimensional governing equations (5), (6), and (12) are

$$\frac{\mathrm{d}\Psi}{\mathrm{d}y^2} = \Upsilon^2 \Psi, \tag{16}$$

$$\rho_{\mathrm{R}} \frac{\partial u}{\partial t} = \mu_{\mathrm{R}} (1 + \eta \mathfrak{D}_t^{\epsilon}) \frac{\partial^2 u}{\partial y^2} + HaE - Ha^2 u + \rho_e + (\rho\alpha)_{\mathrm{R}} Gr\theta, \tag{17}$$

$$(\rho c_p)_{\mathrm{R}} Pr (1 + \lambda \mathfrak{D}_t^c) \frac{\partial \theta}{\partial t} = \nu_{\mathrm{R}} \frac{\partial^2 \theta}{\partial y^2} + Q(1 + \lambda \mathfrak{D}_t^c)\theta. \tag{18}$$

The non-dimensional boundary and initial conditions become

$$\begin{cases} u(y,t) = \theta(y,t) = 0 \quad \text{at} \quad t = 0, \\ \Psi(y) = 1, \quad u(y,t) = 0, \quad \theta(y,t) = 0 \quad \text{at} \quad y = 0, \\ \Psi(y) = R, \quad u(y,t) = 0, \quad \theta(y,t) = 1 \quad \text{at} \quad y = 1, \end{cases} \tag{19}$$

where η is the retardation time, $Ha = HB_y \sqrt{\frac{\sigma}{\mu}}$ is the Hartmann number, λ is the temperature relaxation time, $\mu_{\mathrm{R}} = \frac{\mu_{\mathrm{hnf}}}{\mu_{\mathrm{f}}}$ is the viscosity ratio, $\nu_{\mathrm{R}} = \frac{K_{\mathrm{hnf}}}{K_{\mathrm{f}}}$ is the thermal conductivity ratio, $E = \frac{HE_z}{u_{\mathrm{HS}}} \sqrt{\frac{\sigma}{\mu}}$ is the electric field parameter, $Gr = \frac{\rho g \alpha H^2 (T_1 - T_0)}{\mu u_{\mathrm{HS}}}$ is the Grashof number, $Pr = \frac{c_p \mu}{K_{\mathrm{f}}}$ is the Prandtl number, $Q = \frac{H^2 Q_0}{K_{\mathrm{f}}}$ is the non-dimensional heat source parameter, $R = \frac{\zeta_2}{\zeta_1}$ is the ratio of the zeta potentials, Υ is the Debye-Hükle parameter or electrokinetic parameter, η is the retardation time parameter, and $u_{\mathrm{HS}} = -\frac{\varepsilon \zeta_1 E_x}{\mu}$ is the Helmholtz-Smoluchowski velocity.

3 Method

Under the boundary conditions in Eq. (19), we can solve Eq. (16) and get

$$\Psi = \operatorname{csch}\Upsilon(\sinh(\Upsilon - \Upsilon y) + R\sinh(\Upsilon y)). \tag{20}$$

Then, the charge density will be

$$\rho_e = \Upsilon^2 \operatorname{csch}\Upsilon(\sinh(\Upsilon - \Upsilon y) + R\sinh(\Upsilon y)). \tag{21}$$

The Laplace transformation method is used to get the semi-analytical solution for the velocity and heat fields with the following mathematical form:

$$\bar{u}(y,s) = \int_0^t u(y,t)\mathrm{e}^{-st}\mathrm{d}t. \tag{22}$$

With Eq. (19), applying the Laplace transform formula for the fractional derivative on Eqs. (17), (18), and (19) yields

$$(\rho_{\mathrm{R}} s + Ha^2)\,\bar{u}(y,s) = \mu_{\mathrm{R}}\Big(\frac{\eta\, s}{s+\epsilon(1-s)} + 1\Big)\frac{\partial^2 \bar{u}(y,s)}{\partial y^2} + \frac{Ha\,E}{s} + \frac{\rho_e}{s} + (\rho\alpha)_{\mathrm{R}} Gr\bar{\theta}(y,s), \tag{23}$$

$$\Big(\frac{\partial^2}{\partial y^2} + \frac{1}{\nu_{\mathrm{R}}}(Q - (\rho c_p)_{\mathrm{R}}\, Prs)\Big(\lambda\frac{s}{c(1-s)+s} + 1\Big)\Big)\bar{\theta}(y,s) = 0, \tag{24}$$

$$\begin{cases} \bar{u}(y,t) = 0, \quad \bar{\theta}(y,t) = 0 \quad \text{at} \quad y = 0, \\ \bar{u}(y,t) = 0, \quad \bar{\theta}(y,t) = \dfrac{1}{s} \quad \text{at} \quad y = 1. \end{cases} \tag{25}$$

The analytical solution to Eq. (28) is

$$\bar{\theta}(y,s) = \frac{\operatorname{csch}\sqrt{A(s)}\sinh(\sqrt{A(s)}y)}{s}, \tag{26}$$

where

$$A(s) = \frac{(\rho c_p)_{\mathrm{R}} Prs - Q}{\nu_{\mathrm{R}}}\Big(1 + \frac{\lambda s}{s + c(1-s)}\Big). \tag{27}$$

Applying the finite Fourier sine transform defined in Eq. (42) to Eq. (23) with Eq. (43) yields

$$\tilde{\bar{u}}(\zeta_m, s) = \frac{\overline{A}_1 + s\overline{A}_2}{\mu_{\mathrm{R}}\,\xi_m^2\big(\frac{\eta s^2}{\epsilon(1-s)+s} + s\big) + \rho_{\mathrm{R}} s^2 + Ha^2 s}, \tag{28}$$

where

$$\overline{A}_1 = \frac{1}{\xi_m(\xi_m^2 + \Upsilon^2)}(-HaE\Upsilon^2(\cos\xi_m - 1) + \xi_m^2\Big(- (HaE + \Upsilon^2 R_\zeta)\cos\xi_m + HaE + \Upsilon^2\Big)$$
$$+ \Upsilon^3\xi_m \operatorname{csch}\Upsilon\sin\xi_m(R_\zeta\cosh\Upsilon - 1)), \tag{29}$$

$$\overline{A}_2 = (\rho\alpha)_{\mathrm{R}}\frac{Gr(\sqrt{A(s)}\coth\sqrt{A(s)}\sin\xi_m - \xi_m\cos\xi_m)}{s(A(s) + \xi_m^2)}. \tag{30}$$

Applying the inverse finite sin-Fourier transform defined in Eq. (44) into Eq. (28) yields

$$\bar{u}(y,s) = 2\sum_{m=1}^{\infty}\tilde{\bar{u}}(\zeta_m, s)\sin(\xi_m y), \tag{31}$$

$$\overline{F}(s) = \int_0^1 \bar{u}(y,s)\mathrm{d}y, \tag{32}$$

where $\overline{F}(s)$ is the transformed dimensionless flow rate. We obtain the inverse Laplace transform of the transformed functions (velocity, flow rate, and heat) numerically to get the complete solutions.

4 Numerical solution

In this section, the numerical algorithm is based on the method of the finite difference scheme and will be introduced to solve Eqs. (17) and (18) with the conditions in Eq. (19). Dividing the y domain $[0,1]$ into m grids and the time domain $[0,\overline{T}\,]$ into n grids yields

$$y_i = i\Delta y, \quad t_j = j\Delta t, \tag{33}$$

where $i = 0,1,2,\cdots,m$, $j = 0,1,2,\cdots,n$, $h = 1/m$ is the space step, and $k = \overline{T}/n$ is the time step. We will adopt u_i^j as the numerical solution of $u(y,t)$ at the mesh point (y_i,t_j). To proceed, we consider the following approximations:

$$\frac{\partial u(y,t)}{\partial t}\Big|_i^j = \frac{u_i^{j-1}-u_i^j}{\Delta t} + O(\Delta t), \tag{34}$$

$$\frac{\partial u(y,t)}{\partial y}\Big|_i^j = \frac{u_{i+1}^j - u_{i-1}^j}{2\Delta y} + O(\Delta y^2), \tag{35}$$

$$\frac{\partial^2 u(y,t)}{\partial y^2}\Big|_i^j = \frac{u_{i-1}^j + u_{i+1}^j - 2u_i^j}{\Delta y^2} + O(\Delta y^2). \tag{36}$$

From the Grünwald-Letnikov relation, we have

$$D_t^\alpha [u(y,t)]_i^j = \frac{1}{\Delta t^\alpha}\sum_{k=0}^{j} w_k^\alpha u_i^{j-k}, \tag{37}$$

$$D_t^\beta \Big[\frac{\partial^2 u(y,t)}{\partial y^2}\Big]_i^j = \frac{1}{\Delta t^\beta}\sum_{k=0}^{j}\frac{w_k^\beta (u_{i-1}^{j-k} + u_{i+1}^{j-k} - 2u_i^{j-k})}{\Delta y^2}, \tag{38}$$

where $w_k^\beta = (-1)^k \begin{pmatrix} \beta \\ k \end{pmatrix}$.

Finally, we obtain the following finite difference scheme:

$$\begin{aligned}\rho_{\mathrm{R}}\frac{u_i^n - u_i^{n-1}}{\Delta t} &= A_1 - A_2\, u_i^n + \mu_{\mathrm{R}}\frac{u_{i-1}^n + u_{i+1}^n - 2u_i^n}{\Delta y^2} + \rho_e + Gr(\rho\alpha)_{\mathrm{R}}\theta_i^n \\ &\quad + \eta\mu_{\mathrm{R}}\,\tau^{-\epsilon}\sum_{k=0}^{n}\frac{w_k^\epsilon (u_{i-1}^{n-k} + u_{i+1}^{n-k} - 2u_i^{n-k})}{\Delta y^2},\end{aligned} \tag{39}$$

$$\begin{aligned}&(\rho c_p)_{\mathrm{R}} Pr\Big(\frac{\theta_i^j - \theta_i^{j-1}}{\Delta t} + \lambda\Delta t^{-(c+1)}\sum_{k=0}^{j} w_k^{c+1}\theta_i^{n-k}\Big) \\ &= \nu_{\mathrm{R}}\frac{\theta_{i-1}^j + \theta_{i+1}^j - 2\theta_i^j}{\Delta y^2} + Q\Big(\theta_i^j + \lambda\,\Delta t^{-c}\sum_{k=0}^{j} w_k^c\theta_i^{j-k}\Big),\end{aligned} \tag{40}$$

where $i = 1,2,\cdots,m-1$, and $j = 1,2,\cdots,n$.

The boundary and initial conditions can be discretized by

$$\begin{cases}\theta_i^0 = 0, \quad \theta_0^j = 0, \quad \theta_m^j = 1, \\ u_i^0 = 0, \quad u_0^j = 0, \quad u_m^j = 0,\end{cases} \tag{41}$$

where $i = 0, 1, 2, \cdots, m$, and $j = 0, 1, 2, \cdots, n$.

5 Graphical results and discussion

The semi-analytical and numerical solutions are derived for the EOF of the fractional second-grade hybrid nanofluid through a vertical micro-channel. The effects of the relevant parameters on the electroosmotic velocity, flow rate, and temperature are discussed in this section. The non-dimensional parameters are chosen as follows[3–8,24]:

$$\begin{cases} 0 \leqslant \phi_{\mathrm{T}} \leqslant 6\%, \quad 0 \leqslant Ha \leqslant 10, \quad E = 1, \quad 0 \leqslant Gr \leqslant 4, \quad Pr = 6.2, \\ 0 \leqslant Q \leqslant 4, \quad 0 < R \leqslant 1, \quad 0 \leqslant \Upsilon \leqslant 30, \quad 0 \leqslant \eta \leqslant 1, \quad 0 \leqslant \lambda \leqslant 1. \end{cases}$$

The semi-analytical and numerical solutions for the electroosmotic velocity (u), flow rate (F), and temperature (θ) are shown in Fig. 2. The figure shows that the results are very consistent.

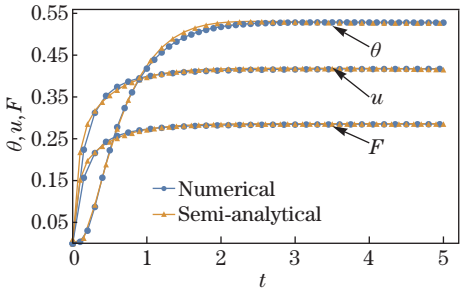

Fig. 2 Semi-analytical and numerical solutions for u, F, and θ when $\phi_{\mathrm{T}} = 6\%$, $\epsilon = 0.8$, $c = 0.8$, $Pr = 6.2$, $\lambda = 0.1$, $Q = 0.5$, $E = 1$, $Ha = 0.5$, $R = 1$, $\eta = 0.1$, $\Upsilon = 2$, and $Gr = 1$ (color online)

5.1 Velocity characteristics

The variations of the electroosmotic velocity (u) and the flow rate (F) for varied values of the volume concentration (ϕ_{T}) where the pertinent parameters are fixed are shown in Fig. 3. It is shown that u and F reach the steady state very quickly. Moreover, an increase in the overall volume concentration (ϕ_{T}) follows by decreasing both u and F due to the change in the momentum of the hybrid nanofluid.

Figure 4 depicts the variations of the electroosmotic velocity and the flow rate under the effect of the fractional-order parameter (ϵ). It can be concluded from the figure that after a short period ($t \leqslant 1$), the elevation of the fractional-order parameter (ϵ) enhances the electroosmotic

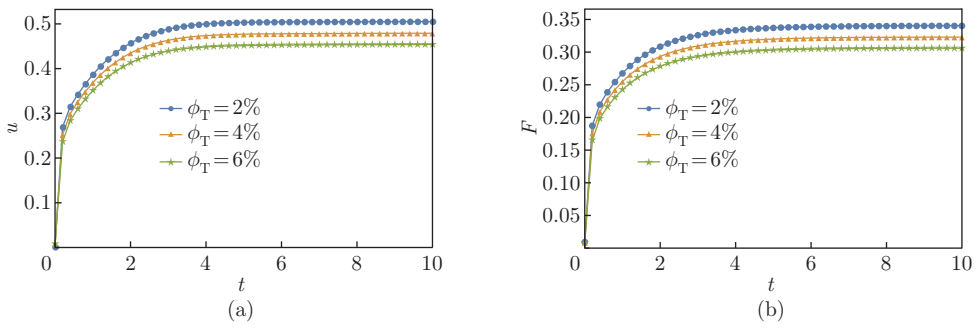

Fig. 3 Variations of (a) u and (b) F versus t for different values of ϕ_{T} when $\epsilon = 0.5$, $c = 0.5$, $Pr = 6.2$, $\lambda = 0.1$, $Q = 0.5$, $E = 1$, $Ha = 0.5$, $R = 1$, $\eta = 0.2$, $Gr = 2$, and $\Upsilon = 2$ (color online)

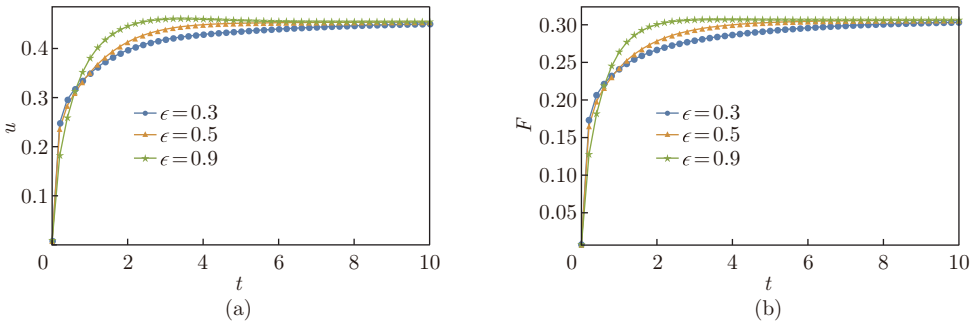

Fig. 4 Variations of (a) u and (b) F versus t for different values of ϵ when $\phi_{\mathrm{T}} = 6\%$, $c = 0.5$, $Pr = 6.2$, $\lambda = 0.1$, $Q = 0.5$, $E = 1$, $Ha = 0.5$, $R = 1$, $\Upsilon = 2$, $Gr = 2$, and $\eta = 0.2$ (color online)

velocity and the flow rate. The main reason is that the fractional-order parameter provides a crucial memory effect on the fluid. Figure 5 shows that an increase in the retardation time (η) delays the electroosmotic velocity and the flow rate to reach the steady state. Physically, a reduction in the retardation time is equivalent to a reduction in the friction, which resists the system elastic deformation.

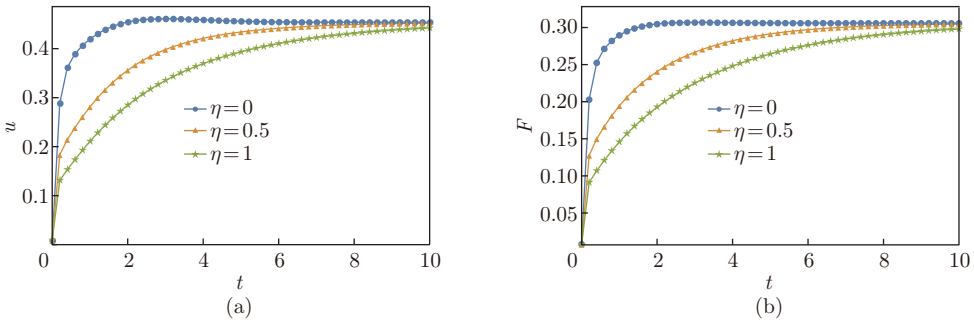

Fig. 5 Variations of (a) u and (b) F versus the time t for different values of η when $\phi_{\mathrm{T}} = 6\%$, $c = 0.5$, $\lambda = 0.1$, $Pr = 6.2$, $Q = 0.5$, $E = 1$, $Ha = 0.5$, $R = 1$, $Gr = 2$, $\Upsilon = 2$, and $\epsilon = 0.5$ (color online)

Figure 6 provides the variations in the electroosmotic velocity with the distance (y) for different values of the Debye-Hükle parameter (Υ). It shows that for small values of the Debye-Hükle parameter, the electroosmotic velocity takes a parabolic shape. In the core flow zone, it exhibits a plug-like profile at higher values, and grows rapidly within the EDL. Physically, the higher the value of Υ, the thinner the Debye layer becomes, resulting in a stronger electroosmotic body force acting on the fluid mass in the EDL, driving the flow. Figure 7 demonstrates the effect of the zeta potential ratio (R) on the electroosmotic velocity. Clearly, in the case of symmetric electrolytes ($R = 1$), the electrostatic velocity takes a symmetric profile. While in the asymmetric case ($R < 1$), the asymmetric electrostatic velocity profile is noticed. This can be justified as higher values of R increase the concentration of ions within the EDL.

The variations of the electroosmotic velocity (u) and the flow rate (F) versus the Hartmann number (Ha) for different values of the Grashof number (Gr) are shown in Fig. 8. It is noticed that u and F increase for small values of Ha while decrease for larger values of Ha. As a result of the small values of Ha, it is seen that the impedance force with the magnitude ($Ha^2\, u$) is smaller than the adding force with the magnitude ($Ha\, E$). However, for the progressive values of Ha, the impedance force is larger than the adding force.

5.2 Temperature characteristics

Figure 9 shows that the elevation of the overall volume concentration (ϕ_{T}) enhances the fluid temperature in the core region of the channel when the thermal conductivity of the hybrid

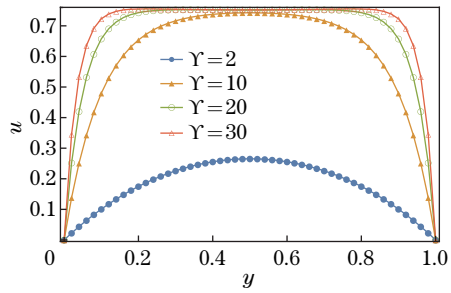

Fig. 6 Variations of u versus y for different values of Υ when $E = 0$, $Ha = 0$, $\phi_{\mathrm{T}} = 2\%$, $c = 0.5$, $Pr = 6.2$, $\eta = 0.8$, $Q = 0.5$, $R = 1$, $\epsilon = 0.5$, $Gr = 0$, and $\lambda = 0.5$ (color online)

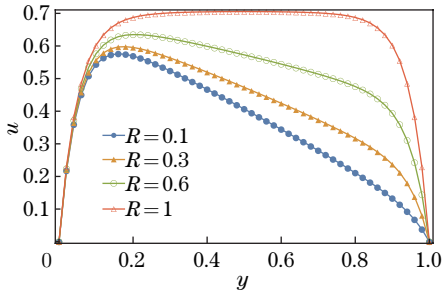

Fig. 7 Variations of u versus y for different values of R when $\phi_{\mathrm{T}} = 6\%$, $c = 0.5$, $\eta = 0.8$, $Pr = 6.2$, $Q = 0.5$, $Ha = 0.5$, $E = 1$, $\epsilon = 0.5$, $Gr = 0$, $\lambda = 0.5$, and $\Upsilon = 20$ (color online)

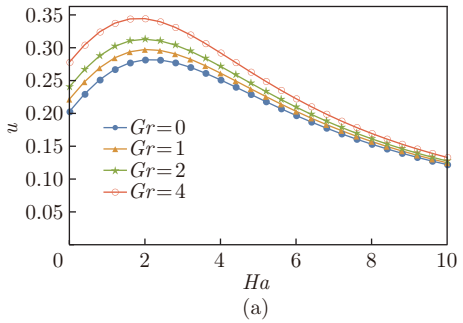

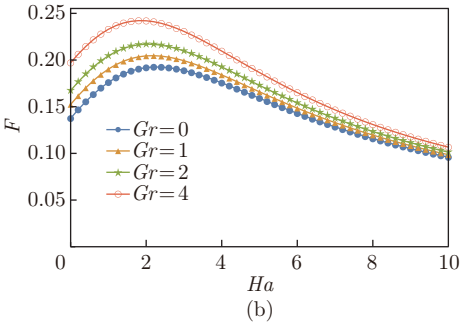

Fig. 8 Variations of u (a) and F (b) versus Ha for different values of Gr when $E = 1$, $\phi_{\mathrm{T}} = 6\%$, $c = 0.5$, $\eta = 0.5$, $Pr = 6.2$, $Q = 0.5$, $R = 1$, $\epsilon = 0.5$, $\lambda = 0.5$, and $t = 1$ (color online)

nanofluid increases. Figure 10 shows the effects of the fractional-order (c) on the temperature evaluated at the centerline of the channel. It is evident that there is a gradual increase in the temperature as time passes by till reaching a steady state. Moreover, the temperature of the hybrid nanofluid is highly dependent on the fractional-order (c) before the steady state.

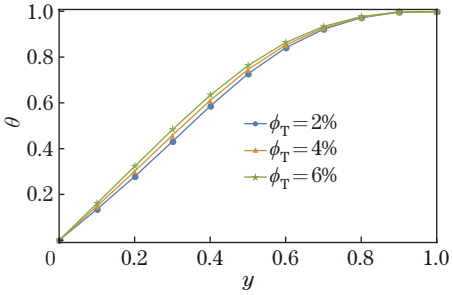

Fig. 9 Effects of ϕ_{T} on θ versus y when $\lambda = 0.8$, $Pr = 6.2$, $Q = 2$, $c = 0.8$, and $t = 1$ (color online)

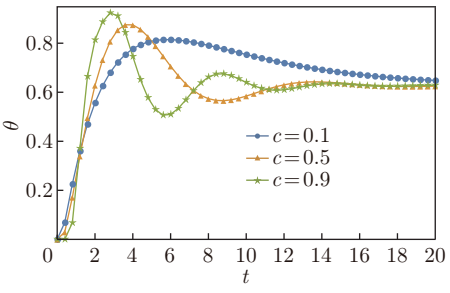

Fig. 10 Effects of c on θ versus t when $\lambda = 1$, $Pr = 6.2$, $Q = 2$, $\phi_{\mathrm{T}} = 6\%$, and $y = 0.5$ (color online)

Figure 11 shows the effects of the relaxation time (λ) on the temperature at the centerline of the channel. It is noticed that the temperature is relaxed at the beginning until a certain value of the time, and then fluctuates. The fluctuation gradually disappears with the increasing time. Figure 12 shows the effects of the heat source parameter on the temperature. It is shown that the temperature fluctuates when the value of the heat source parameter is high, resulting in longer time to reach the steady state.

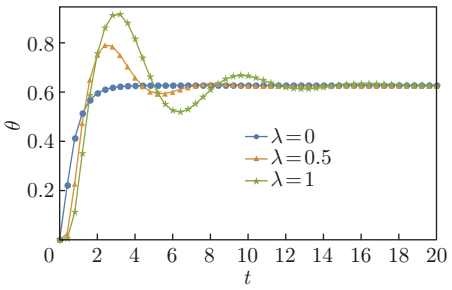

Fig. 11 Effects of λ on θ versus t when $c = 0.8$, $Pr = 6.2$, $Q = 2$, $\phi_T = 6\%$, and $y = 0.5$ (color online)

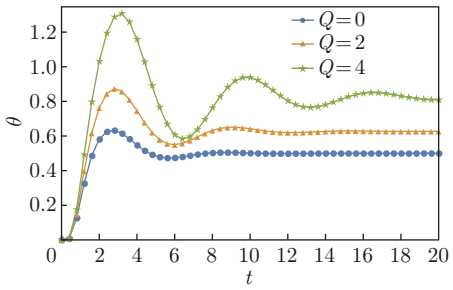

Fig. 12 Effects of Q on θ versus t when $c = 0.8$, $Pr = 6.2$, $\lambda = 0.8$, $\phi_T = 6\%$, and $y = 0.5$ (color online)

Figure 13 depicts the variations of the heat transfer coefficient (Nu) (Nusselt number) through the channel under the effect of the overall volume concentration (ϕ_T). It shows that Nu is enhanced by elevating ϕ_T near the wall ($y = 0$), while this variation vanishes at the core region and inverses near the wall ($y = 1$). Figure 14 shows the effects of the fractional-order (c) on the heat transfer coefficient (Nu) at the wall ($y = 0$). It is clear that the temperature fractional-order highly affects the heat transfer coefficient. Figure 15 depicts the variations of the heat transfer coefficient (Nu) at the wall ($y = 0$) under the effect of the temperature relaxation time (λ). It is noticed that the heat transfer coefficient at the wall ($y = 0$) is relaxed at the beginning of the time period until a certain value of the time, and then fluctuates. The fluctuation gradually disappears with the increasing time. Figure 16 depicts the effects of the heat source parameter on the heat transfer coefficient at the wall ($y = 0$). It is evident that an

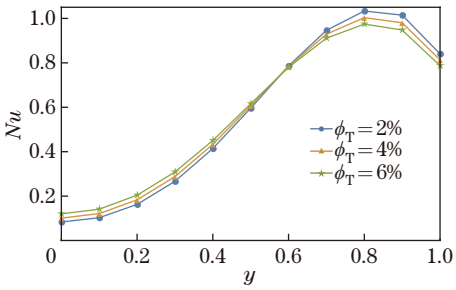

Fig. 13 Variations of Nu versus y for different values of ϕ_T when $Pr = 6.2$, $Q = 2$, $c = 0.8$, $\lambda = 0.8$, and $t = 1$ (color online)

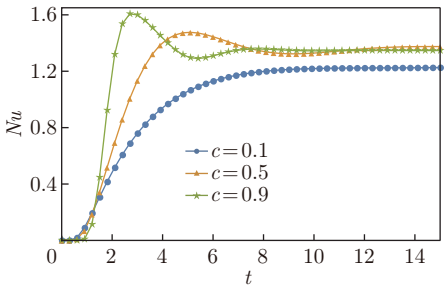

Fig. 14 Variations of Nu versus t for different values of c when $Pr = 6.2$, $Q = 2$, $\phi_T = 6\%$, $\lambda = 0.5$, and $y = 0$ (color online)

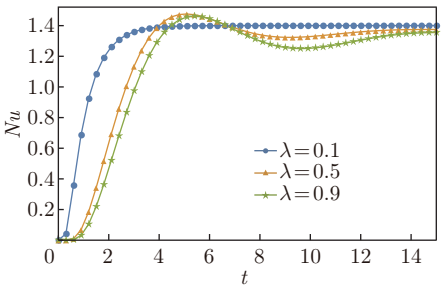

Fig. 15 Variations of Nu versus t for different values of λ when $c = 0.5$, $Pr = 6.2$, $Q = 2$, $\phi_T = 6\%$, and $y = 0$ (color online)

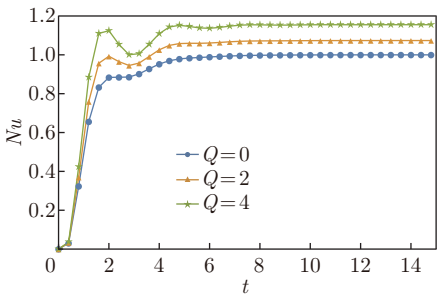

Fig. 16 Variations of Nu versus t for different values of Q when $\lambda = 0.5$, $Pr = 6.2$, $c = 0.5$, $\phi_T = 6\%$, and $y = 0$ (color online)

increase in the heat source will be followed by an increase in the heat transfer coefficient at the wall, but this increment takes a tiny time to appear.

5.3 Validation of results

To validate our results, we prepare Fig. 17 to represent a comparison between the numerical and semi-analytical solutions for the pure fluid, i.e., $\phi_{\mathrm{T}} = 0\%$, with data from Ref. [5]. The figure shows that the current results are very accurate.

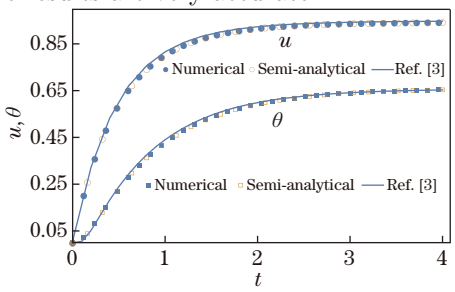

Fig. 17 Data validation when $\phi_{\mathrm{T}} = 0\%$, $\epsilon = 1$, $c = 0$, $Pr = 6.2$, $\lambda = 0$, $Q = 2$, $E = 1$, $Ha = 2$, $R = 1$, $\eta = 0.5$, $Gr = 2$, and $\Upsilon = 10$ (color online)

6 Conclusions

The unsteady EOF of an incompressible fractional second-grade fluid with the low-dense mixture of two distinct spherical nanoparticles, copper, and titanium is examined. The flow of the hybrid nanofluid takes place through a vertical microchannel. A fractional Cattaneo model with heat conduction is also considered. The Lorentz force is responsible for the pressure difference through the microchannel in case of the DC-operated micropump. The Debye-Hükel approximation is utilized to linearize the charge density. The semi-analytical solutions for the velocity and heat equations are obtained with the Laplace and finite Fourier sine transforms and their numerical inverses. In addition to the semi-analytical procedures presented, the numerical algorithm based on the finite difference method is introduced for the given domain. A comparison between the two solutions is presented as well. The results show the following conclusions.

(I) An increase in the overall volume concentration will be followed by a decrease in both the electroosmotic velocity and the flow rate due to the change in the momentum of the hybrid nanofluid.

(II) The fractional-order parameters provide a crucial memory effect on the fluid and temperature fields.

(III) The retardation time parameter delays the electroosmotic velocity and the flow rate to reach the steady state.

(IV) The electroosmotic velocity is supported by the convective force to move the hybrid nanofluid.

(V) The electroosmotic velocity takes a parabolic shape at small values of the Debye-Hükle parameter, while exhibits a plug-like profile in the core flow zone at higher values and grows rapidly within the EDL.

(VI) The overall volume concentration enhances the fluid temperature in the core region of the microchannel due to the increase in the thermal conductivity of the hybrid nanofluid.

(VII) The temperature gradually increases as time passes by reaching the steady state.

(VIII) Higher values of the heat source parameter cause temperature fluctuations and longer time to reach the steady state.

Acknowledgements A. M. ALSHARIF is very pleased with the Taif University Researchers Supporting Project of Taif University of Saudi Arabia (No. TURSP-2020/96).

References

[1] WANG, X. Y., CHENG, C., WANG, S. L., and LIU, S. R. Electroosmotic pumps and their applications in microfluidic systems. *Microfluid Nanofluidics*, **6**, 145–162 (2009)

[2] ZHAO, Q. K., XU, H., and TAO, L. B. Flow and heat transfer of nanofluid through a horizontal microchannel with magnetic field and interfacial electrokinetic effects. *European Journal of Mechanics-B/Fluids*, **80**, 72–79 (2020)

[3] AWAN, A. U., HISHAM, M. D., and RAZA, N. The effect of slip on electro-osmotic flow of a second-grade fluid between two plates with Caputo-Fabrizio time fractional derivatives. *Canadian Journal of Physics*, **97**, 509–516 (2018)

[4] ALSHARIF, A. M. and ABD-ELMABOUD, Y. Electroosmotic flow of generalized fractional second grade fluid with fractional Cattaneo model through a vertical annulus. *Chinese Journal of Physics*, **77**, 1015–1028 (2021)

[5] ABDELLATEEF, A. I., ALSHEHRI, H. M., and ABD-ELMABOUD, Y. Electro-osmotic flow of fractional second-grade fluid with fractional Cattaneo heat flux through a vertical microchannel. *Heat Transfer*, **50**, 6628–6644 (2021)

[6] DEY, P. and SHIT, G. C. Electroosmotic flow of a fractional second-grade fluid with interfacial slip and heat transfer in the microchannel when exposed to a magnetic field. *Heat Transfer*, **50**, 2643–2666 (2021)

[7] WANG, X. P., QI, H. T., YU, B., XIONG, Z., and XU, H. Y. Analytical and numerical study of electroosmotic slip flows of fractional second grade fluids. *Communications in Nonlinear Science and Numerical Simulation*, **50**, 77–87 (2017)

[8] WANG, S. W., ZHAO, M. L., LI, X. C., CHEN, X., and GE, Y. H. Exact solutions of electroosmotic flow of generalized second-grade fluid with fractional derivative in a straight pipe of circular cross section. *Zeitschrift für Naturforschung A*, **69**, 697–704 (2014)

[9] ABDELSALAM, S. I., VELASCO-HERNÁDEZ, J. X., and ZAHER, A. Z. Electromagnetically modulated self-propulsion of swimming sperms via cervical canal. *Biomechanics and Modeling in Mechanobiology*, **20**, 861–878 (2021)

[10] ABDELSALAM, S. I. and ZAHER, A. Z. Leveraging elasticity to uncover the role of Rabinowitsch suspension through a wavelike conduit: consolidated blood suspension application. *Mathematics*, **9**, 1–25 (2021)

[11] BHATTI, M. M. and ABDELSALAM, S. I. Bio-inspired peristaltic propulsion of hybrid nanofluid flow with tantalum (Ta) and gold (Au) nanoparticles under magnetic effects. *Waves in Random and Complex Media* (2021) https://doi.org/10.1080/17455030.2021.1998728

[12] BHATTI, M. M. and ABDELSALAM, S. I. Thermodynamic entropy of a magnetized Ree-Eyring particle-fluid motion with irreversibility process: a mathematical paradigm. *ZAMM-Zeitschrift für Angewandte Mathematik und Mechanik*, **101**, e202000186 (2021)

[13] QI, H. T., XU, H. Y., and GUO, X. W. The Cattaneo-type time fractional heat conduction equation for laser heating. *Computers and Mathematics with Applications*, **66**, 824–831 (2013)

[14] XU, G. Y. and WANG, J. B. Analytical solution of time fractional Cattaneo heat equation for finite slab under pulse heat flux. *Applied Mathematics and Mechanics* (*English Edition*), **39**(10), 1465–1476 (2018) https://doi.org/10.1007/s10483-018-2375-8

[15] XU, X. Y., QI, H. T., and JIANG, X. X. Fractional Cattaneo heat equation in a semi-infinite medium. *Chinese Physics B*, **22**, 0114401 (2013)

[16] ANANTHA-KUMAR, K., RAMANA-REDDY, J. V., SUGUNAMMA, V., and SANDEEP, N. MHD Carreau fluid flow past a melting surface with Cattaneo-Christov heat flux. *Applied Mathematics and Scientific Computing. Trends in Mathematics*, Birkhäuser, Cham (2019)

[17] RAMANDEVI, B., RAMANA-REDDY, J. V., SUGUNAMMA, V., and SANDEEP, N. Combined influence of viscous dissipation and non-uniform heat source/sink on MHD non-Newtonian fluid flow with Cattaneo-Christov heat flux. *Alexandria Engineering Journal*, **57**, 1009–1018 (2018)

[18] ANANTHA-KUMAR, K., RAMANA-REDDY, J. V., SUGUNAMMA, V., and SANDEEP, N. Magnetohydrodynamic Cattaneo-Christov flow past a cone and a wedge with variable heat source/sink. *Alexandria Engineering Journal*, **57**, 435–443 (2018)

[19] TRIPATHI, D., PRAKASH, J., TIWARI, A. K., and ELLAHI, R. Thermal, microrotation, electromagnetic field and nanoparticle shape effects on Cu-CuO/blood flow in microvascular vessels. *Microvascular Research*, **132**, 104065 (2020)

[20] ELELAMY, A. F., ELGAZERY, N. S., and ELLAHI, R. Blood flow of MHD non-Newtonian nanofluid with heat transfer and slip effects: application of bacterial growth in heart valve. *International Journal of Numerical Methods for Heat & Fluid Flow*, **30**, 4883–4908 (2020)

[21] RIAZ, A., BOBESCU, E., RAMESH, K., and ELLAHI, R. Entropy analysis for cilia-generated motion of Cu-blood flow of nanofluid in an annulus. *Symmetry*, **13**, 2358 (2021)

[22] KHAN, U., SHAFIQ, A., ZAIB, A., and BALEANU, D. Hybrid nanofluid on mixed convective radiative flow from an irregular variably thick moving surface with convex and concave effects. *Case Studies in Thermal Engineering*, **21**, 100660 (2020)

[23] CHRISTOPHER, A. J., MAGESH, N., GOWDA, R. J. P., KUMAR, R. N., and KUMAR, R. S. V. Hybrid nanofluid flow over a stretched cylinder with the impact of homogeneous-heterogeneous reactions and Cattaneo-Christov heat flux: series solution and numerical simulation. *Heat Transfer*, **50**, 3800–3821 (2021)

[24] EL-MASRY, Y., ABD-ELMABOUD, Y., and ABDEL-SATTAR, M. A. Direct current/alternating current magnetohydrodynamic micropump of a hybrid nanofluid through a vertical annulus with heat transfer. *Journal of Thermal Science and Engineering Applications*, **12**, 044501 (2020)

[25] EZZAT, M. A. Thermoelectric MHD non-Newtonian fluid with fractional derivative heat transfer. *Physica B*, **405**, 4188–4194 (2010)

[26] ABD-ELMABOUD, Y. Electroosmotic flow of generalized Burgers' fluid with Caputo-fabrizio derivatives through a vertical annulus with heat transfer. *Alexandria Engineering Journal*, **59**, 4563–4575 (2020)

Appendix A

Let $g(y)$ be a continuous or piecewise continuous function in an interval $(0 < y < 1)$. The finite Fourier sine transform of $g(y)$ is defined by

$$\mathfrak{F}\{g(y)\} = \tilde{g}(\xi_m) = \int_0^1 g(y)\sin(\xi_m y)\mathrm{d}y \tag{A1}$$

with

$$\mathfrak{F}\{g''(y)\} = -\xi_m^2\tilde{g}(\xi_m) + \xi_m(g(0) + (-1)^{m+1}g(1)). \tag{A2}$$

The inverse finite sine Fourier transform is

$$\mathfrak{F}^{-1}\{\tilde{g}(\xi_m)\} = 2\sum_{m=1}^{\infty}\tilde{g}(\xi_m)\sin(\xi_m y), \tag{A3}$$

where ξ_m are the positive roots of the transcendental equation $\tan\xi_m = 0$.